FRONTIERS OF PHYSICS

TOPICAL REVIEW
Volume 19 / Issue 6 / 62500 / 2024

Recent advances of light-field modulated operation in laser-induced breakdown spectroscopy

Shangyong Zhao[1,†], Yuchen Zhao[2], Yujia Dai[1], Ziyuan Liu[1], Huihui Zha[1], Xun Gao[3,4,‡]

1 College of Opto-Electro-Mechanical Engineering, Zhejiang A & F University, Hangzhou 311300, China
2 Nottingham University Business School China, University of Nottingham Ningbo China, Ningbo 315100, China
3 School of Science, Changchun University of Science and Technology, Changchun 130022, China
4 Ministry of Education Key Laboratory for Cross-Scale Micro and Nano Manufacturing, Changchun University of Science and Technology, Changchun 130022, China
Corresponding authors. E-mail: †syzhao@zafu.edu.cn, ‡lasercust@163.com
Received March 26, 2024; accepted June 24, 2024

ABSTRACT

The simplicity and low-cost way to improve qualitative and quantitative analytical performance has always been a crucial concern for laser-induced breakdown spectroscopy (LIBS), and many scientists have been engaged in this evolving research direction. In this review, we investigated an update on recent developments in light-field modulated operation in LIBS. It covered a brief description of LIBS, optical polarization, and beam shaping. Here, the optical polarization is divided into laser beam polarization and plasma polarization. In addition, the methodology and development of light-field modulated LIBS were summarized and discussed. Finally, the existing problems with light-field modulated LIBS were presented, along with some of their own insights and the future direction of their development. This review will provide a guideline for LIBS researchers with basic knowledge, which is very useful in the signal optimization of LIBS research and applications.

Keywords laser-induced breakdown spectroscopy, light-field modulated, laser beam polarization, plasma polarization, beam shaping

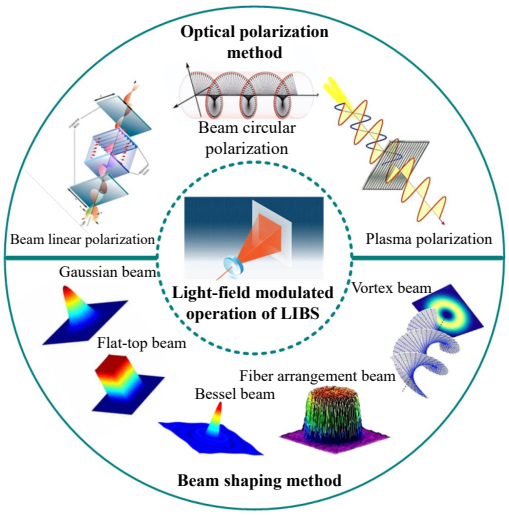

Contents

Higher Education Press

https://doi.org/10.1007/s11467-024-1436-1

1 Introduction

Laser-induced breakdown spectroscopy (LIBS) has the advantages of rapid, *in-situ*, multi-element detection, remote operation, and safety, and is regarded as the "future superstar for chemical analysis" [1]. However, due to the signal instability, higher background, and lower sensitivity, the popularization, industrialization, and commercialization progress of LIBS was very slow [2]. The essential feature of LIBS measurement objects is a dynamically changing laser plasma, which exhibits rapid expansion and spatial variability in the microsecond-level time delay range. Laser-produced plasma optimization has been the focus of academics and researchers for many years. Several optimization solutions have been proposed, including double-pulse [3], spark discharge pulse re-excitation [4], microwave supplementary [5], resonance excitation [6], flame supplementary [7], cavity confinement [8], magnetic field confinement [9], nanoparticle and micro-nanostructure [10, 11], external gas and pressure [12, 13], light-field modulated [14–16], ultrafast laser beam [17], sample's physical property [18, 19], and technology combined (nanoparticles double-pulse, external gas magnetic field confinement, cavity magnetic field confinement, etc.) [20–22]. Comparatively, the light-field modulated operation method is one of the optimization solutions that is most capable of building simplicity and a low-cost way to improve LIBS qualitative and quantitative analysis abilities.

There are two major implementation schemes of light-field modulated operation: one is laser beam polarization and shaping, and the other is plasma polarization. The former is based on a laser beam with a particular phase or polarization distribution to increase the laser ablation and improve plasma emission signal intensity, while the latter is based on the differences in polarization principles between continuous and discrete spectra to reduce background signal interference. As reported so far, the light-field modulated operation contains the flat-top beam [23], vortex beam [24], Bessel beam [25], optical fiber configuration [26], linear polarization, and circular polarization [27, 28]. Those methods can optimize the source signal, which resulted in the improvement of LIBS qualitative and quantitative analysis abilities and an increase in accuracy and reliability. Generalizing those methods and experiences of the light-field modulated operation of LIBS, comparing and analyzing the methods, and seeking the general and difference character to supply theoretical and data bases, however, the overview knowledge has been reported rarely.

In this review, we aim to investigate the qualitative and quantitative performance improvement of LIBS by light-field modulated operation. It covers a brief description of the laser plasma process, laser beam polarization, laser beam shaping, and evaluation parameters. Additionally, a summary and discussion of the methodology and application of optical polarization and beam shaping are provided. Finally, conclusions and perspectives on the light-field modulated operation of LIBS are presented.

2 Fundamental principle

2.1 Laser plasma process

The schematic diagram of the laser plasma process and spectral analysis is shown in Fig. 1. A typical LIBS setup includes a high-power laser, spectrometer, digital delay generator, translation stage, and optical device [29]. When a high-power pulsed laser beam is focused on the irradiating sample surface, the laser plasma will be generated via a series of physical processes including melting, evaporation, expression, cooling, and vanishing [30]. The elemental composition and content information of the measured sample can be derived by analyzing the plasma emission spectra [31].

The two pivotal steps in the LIBS process are laser ablation and plasma signal acquisition. In the early stage of plasma expansion, temperature fluctuation contributes most to signal uncertainty, and the total particle population density fluctuation contributes the most to the signal uncertainty from ~800 ns. It may already be heading towards a predictable conclusion that the total particle population density fluctuation contributes the most to the signal uncertainty of LIBS measurement [32, 33]. The time-resolved LIBS plasma images and spectra show that the images are stable in the early stage of LIBS plasma evolution but unstable in the late stage, and the LIBS signal's uncertainty decreases first and then increases. The reason for signal uncertainty comes from two aspects [33, 34]: (i) the large contribution of early temperature fluctuations is essentially due to the high background noise caused by electron bremsstrahlung, which affects temperature calculation; and (ii) the fluctuation of the total particle number density is mainly because of the instability of the plasma's spatial shape. The light-field modulated operation is aimed at laser ablation and plasma emission signal procedures to improve the overall signal intensity and reduce background noise.

2.2 Optical polarization

2.2.1 Laser beam polarization

In light-field modulated LIBS operation, the laser beam polarization usually involves linear polarization and circular polarization [28]. In most cases, the beam of light emitted by the laser is linearly polarized; that is, the electric field oscillates in a specific direction perpendicular to the propagation direction of the laser beam,

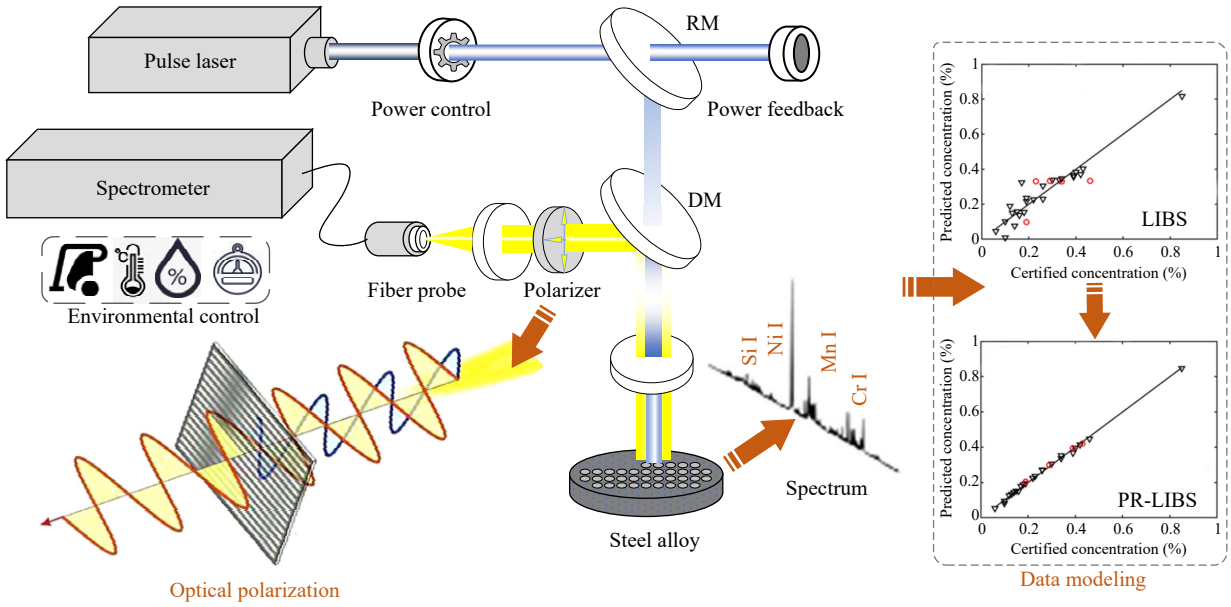

Fig. 1 Schematic illustration of polarization-resolved LIBS system configuration [35].

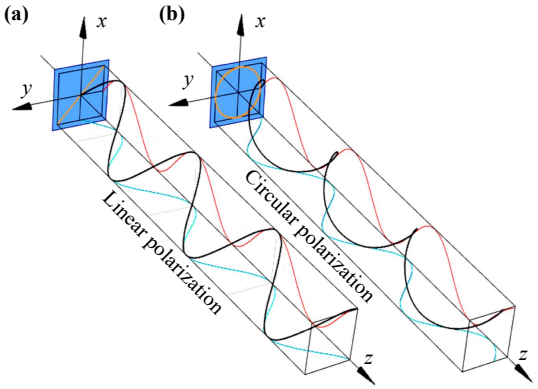

Fig. 2 Schematic diagram of linear polarization **(a)** and circular polarization **(b)**.

as shown in Fig. 2(a). Some lasers, like fiber lasers, do not produce linearly polarized light, but there are other stable polarization states that can be converted into linearly polarized light using a suitable combination of wave plates. A linear polarization can be transformed into a circular polarization when the line-type beam enters a $\lambda/4$ plate or phase retarder, as shown in Fig. 2(b) [27]. A wave plate can introduce a phase difference, thereby converting linear polarization into circular polarization for the laser beam. The laser beam polarization state would affect the absorptivity of the material surface, which in turn affects the ablation amount during the laser-matter interaction process [28].

The conventional linearly polarized laser beam, the elliptically polarized laser beam, and the circularly polarized laser beam are all scalar light fields. The polarization state is evenly distributed due to the evenly distributed direction of the electric vector on the beam cross section. Generally, a polarized laser beam whose polarization direction is perpendicular to the incident plane is called s-polarization, while p-polarization refers to one whose polarization direction is parallel to the incident plane. Besides, the radially polarized laser beam and the angular polarized laser beam are novel types of laser beams with unique polarization modes. Its polarization type is quite different from that of conventional linearly or circularly polarized laser beams. The polarization distribution of the same wave front is different at different positions at the same time, and the polarization direction changes with the spatial position.

2.2.2 Plasma polarization

As mentioned previously, the laser beams used in LIBS, such as nanosecond (ns) and femtosecond (fs) laser devices, are normally linearly polarized. The laser plasma emission spectra can be broadly classified into four categories despite their complicity: continuous background emission signal, noise signal, ion emission spectra, and atomic emission spectra [27, 35]. In the early stages of laser plasma generation, plasma emission mechanisms are mainly blackbody and bremsstrahlung radiation, which produce ultraviolet, visible, and continuous spectra. With the rapid expansion and diffusion of the plasma, the plasma temperature and electron density sharply drop, and submerged discrete spectral lines begin to appear, mainly the transition radiation between electrons and ions. The LIBS signal detection window still has stronger background noise [36]. Based on the diversity between background spectra and discrete spectra, it has been confirmed that both of them are polarized in the plasma spectrum, and there are

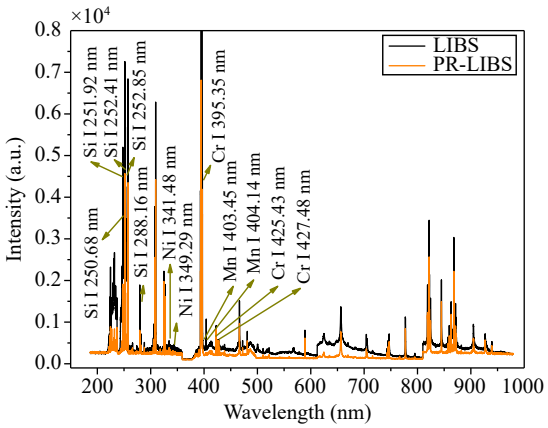

Fig. 3 Comparison of LIBS and PR-LIBS spectra [35].

differences in polarization degree and polarization direction [35]. A comparison of LIBS and polarization-resolved LIBS (PR-LIBS) has been shown in Fig. 3. Through the polarization device, regulation can be realized to weaken the influence of background and improve the detection window signal stability, and usually a linear polarizer is used in the spectral acquisition process.

2.3 Laser beam shaping

The current laser beam spot used in the LIBS system presents a Gaussian distribution, but the energy distribution of the laser beam is not perfect [37]. The Gaussian distribution results in an uneven energy distribution because there is too much intermediate energy, and the outer boundary is usually underpowered. This can cause an "unstable weld puddle" condition and compromise the LIBS signal's stability. Laser beam shaping is the process of converting a laser beam into a specific pattern, shape, or intensity distribution to optimize LIBS detection performance. Common beam shaping operations include flat-top beam [38], Bessel beam [39], vortex beam [40], and fiber arrangement shaping [41]. The simulation morphology of the Gaussian beam, flat-top beam, Bessel beam, fiber arrangement shaping, and vortex beam is shown in Figs. 4(a)–(e).

2.4 Evaluation parameter

2.4.1 Plasma parameter

According to the local thermodynamic equilibrium (LTE) assumption with an optically thin condition, the plasma temperature $T(t)$ can be given by the Boltzmann plot method, as follows [42]:

$$\ln\frac{I_{\lambda_{i,j}}}{g_i A_{i,j}} = -\frac{E_i}{k_{\mathrm{B}} T_{(t)}} + \ln\left(\frac{hcN_Z}{4\pi U\left(T(t)\right)}\right), \tag{1}$$

where $I_{\lambda_{i,j}}$ is the spectral intensity, g_i is the upper level degeneracy, $A_{i,j}$ is the electron transition probability, E_i is the upper level energy, k_{B} is the Boltzmann constant, $T(t)$ is the time-resolved plasma temperature, h is the Plank constant, c is the speed of light, N_Z is the atomic number density in plasma, and $U(T(t))$ is a partition function at the corresponding temperature.

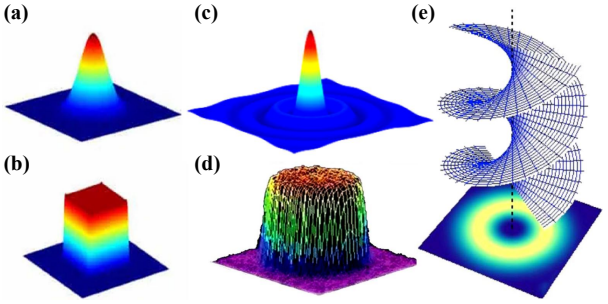

Fig. 4 Laser beam morphology: **(a)** Gaussian beam, **(b)** flat-top beam, **(c)** Bessel beam, **(d)** fiber arrangement shaping, and **(e)** vortex beam.

The electron density is related to the spectral broadening width of the emission line, and the main spectrum broadening is from the Stark effect. The electron density n_e can be calculated as follows [43]:

$$\Delta_{\lambda_{1/2}} = 2\omega n_e 10^{-16}, \tag{2}$$

where $\Delta_{\lambda_{1/2}}$ is the full width at half maximum (FWHM), and ω is the electron impact parameter.

2.4.2 Evaluation indexes

To assess the optimistic effect of the light-field modulated operation of the LIBS approach, the signal-to-background ratio (SBR), relative standard deviation (RSD), coefficient of determination (R^2), mean absolute error (MAE), root-mean-square error ($RMSE$), and enhancement factor (EF) are commonly used to evaluate the optimization performance of the light-field modulated operation of previous work, as listed in Table 1.

3 Methodology and results

3.1 Optical polarization method

3.1.1 Polarization laser ablation

As mentioned earlier, laser beam polarization consists of linearly (p-polarization, s-polarization, or others), circularly, radially, and angularly polarized laser beams. Polarization laser ablation mainly focuses on the damage morphology (zero crater size), hole depth, and ablation rate and helps to compare the differences between polarization angles [49–52] or polarization types [53], as shown in Fig. 5. For linearly polarized laser beams, the

Table 1 Evaluation indexes used in a quantitatively analytical approach (I_B is the background signal intensity, δ is the standard deviation, x is the corresponding average value, SSR is the sum of squares of residuals, SST is the total sum of squares, y_i and y_i' are the predicted and measured values, respectively, I and I_0 are the raw and optimized spectral intensities, respectively, and S is the slope of the standard curve).

Index	Expression	Description	Ref.
SBR	$SBR = I_B/I$	A parameter to evaluate the optimization effect of feature signal.	[44]
RSD	$RSD = (\delta/\overline{x}) \times 100\%$	The degree of dispersion of the data set relative to its mean.	[45]
R^2	$R^2 = 1 - (SSR/SST)$	Reflects the goodness of fit between regression line and sample observations.	[46]
MAE	$MAE = \int ((\lvert y_i - y_i' \rvert)/m)$	The average difference between the predicted value and the true value.	[47]
$RMSE$	$RMSE = sqrt\,(MSE)$	The difference between the predicted value and the actual measured value.	[46]
EF	$EF = I/I_0$	The feature spectral lines intensity enhancement times value.	[48]
LOD	$LOD = 3\delta/S$	An analytical method can detect a minimum concentration in a sample.	[3]

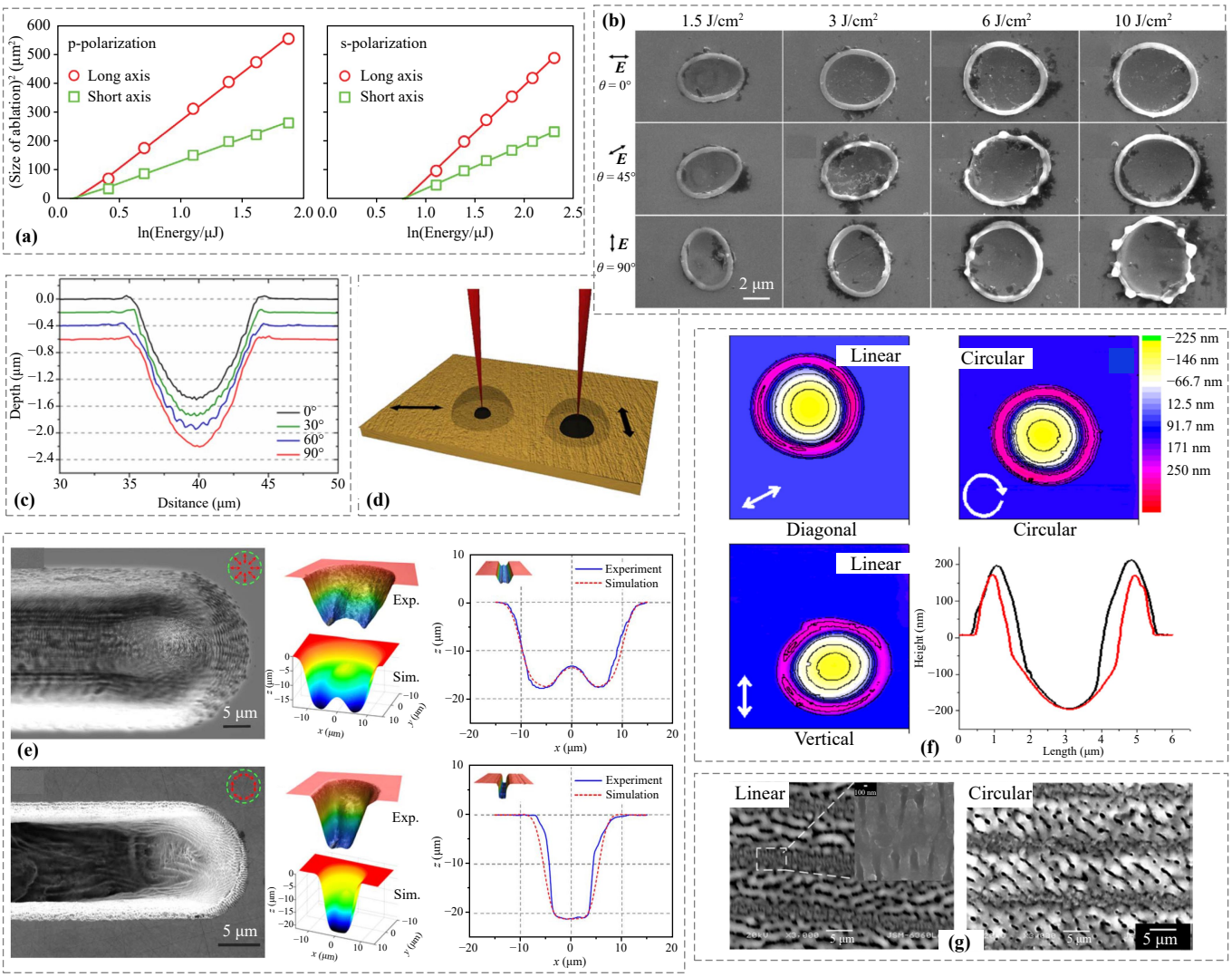

Fig. 5 Polarization laser ablation results: **(a)** p-polarization and s-polarization [56], **(b)** damage morphology [51], **(c)** hole depth [52], **(d)** polarization direction [58], **(e)** radially and angularly polarized laser beam [63], **(f)** simulation of linearly and circularly polarized laser beam ablation [66], and **(g)** horizontally and circularly polarized laser ablation [53].

ablation rate and radius vary periodically with polarization angle [54, 55], and the zero crater sizes of p-polarization and s-polarization are different at the same laser energy and beam incidence angle [56, 57] [Fig. 5(a)]. The ablation process of the incident laser pulse with an electric field aligned perpendicular to the linear surface feature is

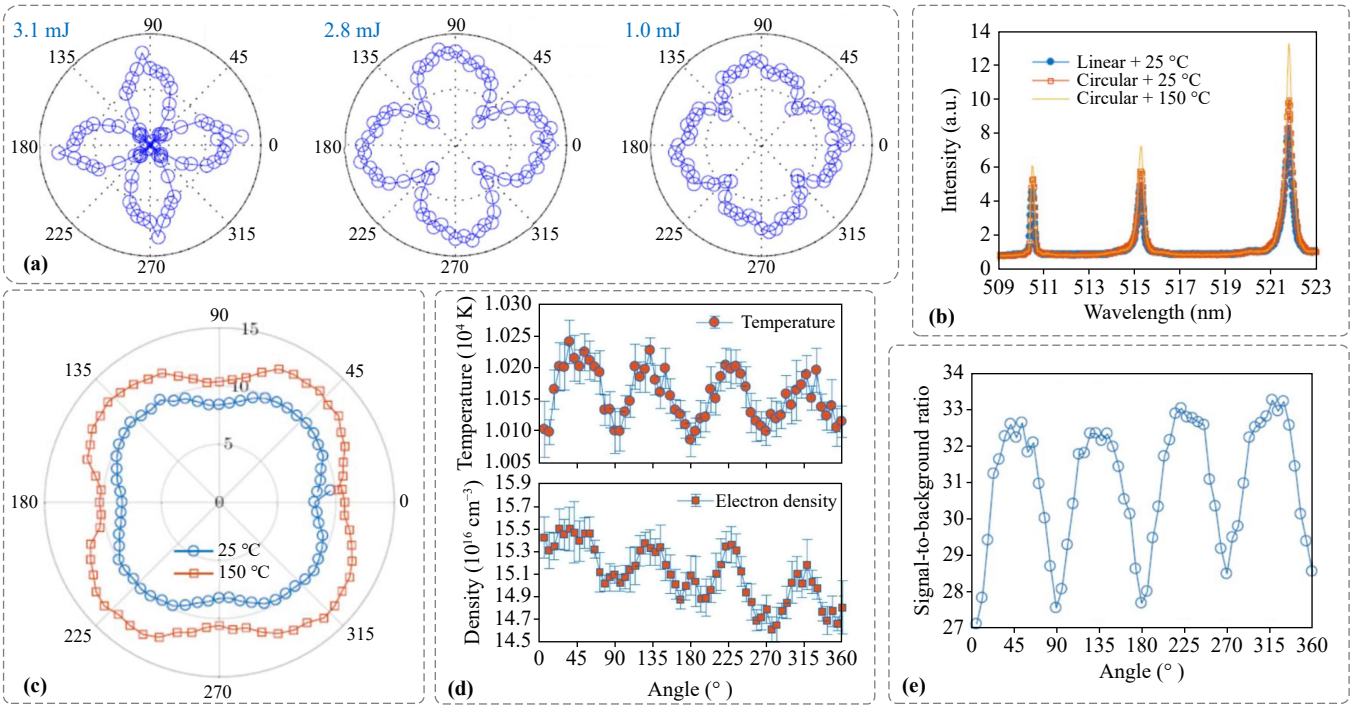

Fig. 6 Typical results of the laser beam polarization method of LIBS: **(a)** Polarization-resolved signal intensity [74], **(b, c)** temperature-related linear-circular polarization signal intensity [28], **(d)** polarization-resolved plasma temperature and electron density [28], and **(e)** polarization-resolved *RSD* [28].

weaker compared with the parallel orientations [58] [Fig. 5(d)]. For linear (p-polarization, s-polarization) and circular laser beams, the differences in surface structure damage morphology and hole depth can be observed very intuitively [59–62]. The polarization effects of radially and angularly polarized laser beams have different ablated cross-sectional profiles [63–65], as shown in Fig. 5(e). For linear polarization, the heated zone is elongated in the polarization direction, and the thermal gradient on the major axis (from center to boundary) is much larger. But for circular polarization, the heated zone is circular, with less variation than linear polarization [66], as shown in Fig. 5(f).

3.1.2 Laser beam polarization-resolved LIBS

The current laser beam polarization focuses mainly on the qualitative analysis of linear polarization and circular polarization. It radiates into several research directions, as follows: (i) polarization-resolved physical properties of plasma (signal intensity, plasma temperature, and electron density) [28, 67–69]; (ii) linear-circular polarization comparison [28, 69–71]; (iii) polarized atomic, ionic, and molecule signal characteristics [27, 71–74]; and (iv) technology combined [3, 75]. The typical results of the laser beam polarization method are shown in Fig. 6. The LIBS signal, plasma temperature, and electron density presented regular changes in strength and weakness with polarization angle [28, 74]. Besides, the spectral signal intensity and stability of the circular polarization case are better than those of linear polarization [69]. Finally, laser beam polarization combined with other optimization methods like sample temperature and ambient pressure changes can further improve the LIBS performance [28, 75].

3.1.3 Plasma polarization-resolved LIBS

Among the plasma polarization characteristic research, the polarizing angle [27, 76], laser energy [77, 78], polarization recognition rate [79, 80], laser pulse width [81], feature lines [82, 83], delay time [84, 85], polarization state (s-wave and p-wave) [86], plasma temperature and electron density [87], polarizer types [85], and spectral line abundance [88] are investigated. However, whether the plasma polarization method can effectively control the background noise and improve *SBR* remains controversial [87, 89].

In addition to all the above, some researchers have now proposed a plasma polarization method that can be realized in LIBS quantitative analysis and identification ability improvement. The summary and comparison of experimental results using the plasma polarization method are shown in Table 2. Zhao *et al.* [90] proposed PR-LIBS combined with support vector regression to improve the accuracy of soil heavy-metal (Cd) detection. Compared to LIBS, the R^2 increased to 0.9946, the *RMSEC* decreased by 11.8783 μg/g, and the *RMSEP*

Table 2 The summary and comparison of experimental results.

Sample	*Ele.*	*RSD*		R^2		*RMSE*		Ref.
		LIBS	PR-LIBS	LIBS	PR-LIBS	LIBS	BS-LIBS	
Soil	Cd	5.26%	4.8%	0.9642	0.9841	50.3812	32.9196	[90]
Steel alloys	Si	9.2%	5.9%	**0.912**	**0.970**	0.070	0.050	[35]
	Mn	7.7%	5.5%	0.904	0.953	**0.030**	**0.020**	
	Cr	**9.3%**	**6.0%**	0.965	0.996	1.150	0.790	
	Ni	7.2%	5.8%	0.952	0.986	0.840	0.680	
Steel sample	Cr	–	–	0.97876	0.99291	–	–	[91]
	Cu			0.97704	0.98829			
	Pb			0.98432	0.99603			
	Fe			0.98202	0.99299			

decreased by 11.8906 μg/g. Zhao *et al.* [35] investigated the stability and accuracy improvement of Si, Mn, Cr, and Ni element analysis in steel alloys by PR-LIBS, and found that the *RSD* and *RMSE* of PR-LIBS decreased while the *SBR* and R^2 increased compared to LIBS. For the PR-LIBS dataset, the R^2 has increased by at least 3.4%, and the *RMSEC* and *RMSEP* have improved by at least 6.3% and 19.0%, respectively. Xu *et al.* [91] applied the micro-linear spectra model (MLS) to improve the stability of LIBS for chromium in soil, and the results showed that the stability of MLS increased by 3.9% compared with the recognition curve of LIBS. Besides, Teng *et al.* [92] investigated full-Stokes polarization laser-induced breakdown spectroscopy detection of infiltrative glioma boundary tissue. They concluded that PR-LIBS provides more complete polarization information and elemental information than conventional LIBS elemental analysis, and Stokes parameter spectra can significantly reduce the under-fitting phenomenon of artificial intelligence identification models.

3.2 Laser beam shaping method

3.2.1 Beam shaping laser ablation

The traditional Gaussian beam energy follows a Gaussian distribution, and the laser-focused spot is irradiated on the measurement area of the target material, resulting in inaccurate energy distribution and low laser ablation efficiency. Unlike Gaussian beams, taking a flat top beam as an example, the energy distribution of a flat top beam has a clear size and shape, the intensity of the entire spot is uniform, the edges are sharp, and there is no energy outside the spot area, which is opposite to the continuous attenuation of Gaussian beams [93]. Other technologies, such as Bessel beams, vortex beams, and spot arrays, have also been widely applied and studied [94–99]. Yin *et al.* [100] compared the evaporation ablation dynamics of materials by the nanosecond pulse laser with a Gaussian beam [Fig. 7(a)] and a flat-top beam [Fig. 7(b)]. For the Gaussian beam, the center of the target is first ablated, followed by radial ablation, whereas for the flat-top beam, the lower energy density after beam shaping results in a delay in the evaporation time of the target surface. Besides, the center of the crater produced by the Gaussian beam is deep and shallow on both sides, while the craters generated by the flat-top beam are relatively flat. Different energy distributions and coupling efficiencies will lead to various morphologies of the target ablation [Fig. 7(c)] [101]. Burger *et al.* [102] examined the utility of Gaussian and structured (Laguerre–Gaussian, Airy, and Bessel–Gaussian) beam shaping on femtosecond filament-induced breakdown spectra in the nonlinear regime [Fig. 7(d)]. The ablation profiles qualitatively correspond to the intensity profiles in the linear regime [102, 103]. Ackermann *et al.* [104] studied phase-only beam shaping with a spatial light modulator (SLM), which enables the shaped profile to adapt to the ablation geometry, thereby tailoring the energy deposition. Pallarés-Aldeiturriag *et al.* [105] found that the average surface roughness obtained by deploying the cylindrical vector was reduced to 94% compared to the Gaussian case, and the processing efficiency was improved by 80%. It is worth mentioning that beam shaping laser ablation can also precisely control the area, shape, and depth [Figs. 7(d)–(f)] [106–112].

3.2.2 Beam shaping-assisted LIBS

Beam shaping-assisted LIBS (BS-LIBS) applies a binary optical device (amplitude or phase type device) to modulate the wave front amplitude or phase of the laser spot, and furthermore changes the laser plasma spatial morphology, stability, and radiation signal intensity [113]. The diffractive optical element (DOE) is the key component in BS-LIBS. The embossed structure with different depths is etched on the surface of the optical material substrate by surface micro-machining technology, and the laser beam wavefront amplitude or phase is modulated when a laser beam passes through the DOE. The summary and comparison of the evaluation index and laser plasma parameter results of previous work are listed in Table 3. In Table 3, there are three types of

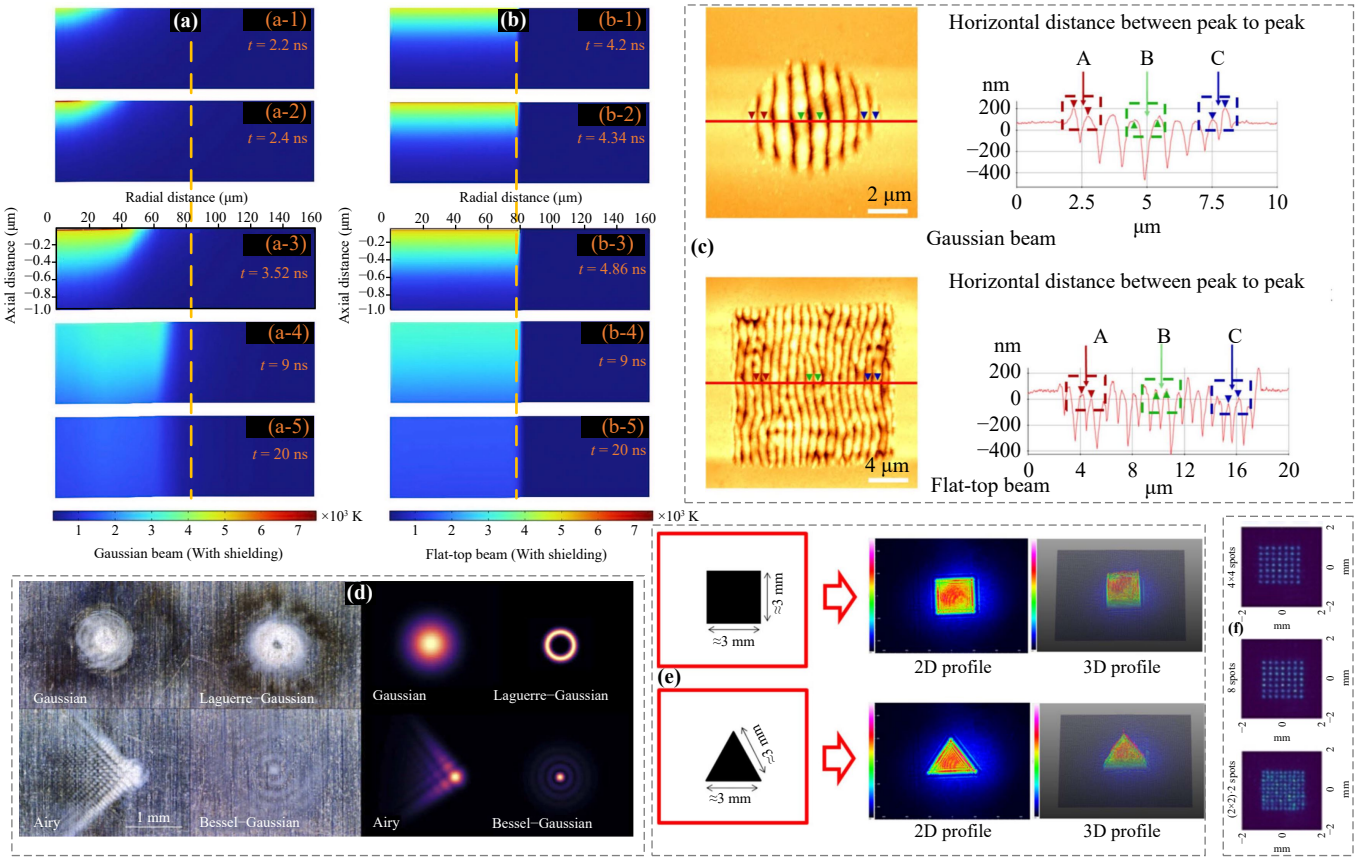

Fig. 7 Beam shaping laser ablation results: **(a)** Gaussian beam [100], **(b)** flat-top beam [100], **(c)** Gaussian beam and flat-top beam ablation surface [101], **(d)** Gaussian beam, Laguerre–Gaussian beam, airy beam, and Bessel–Gaussian beam [102], **(e)** square and triangular beams [107], and **(f)** spot arrays [97].

Table 3 The summary and comparison of experimental and plasma parameters (Gaussian beams are generally used for LIBS).

Sample	Beam type	*Ele.*	*RSD*		R^2		*LOD* (ppm)		Ref.
			LIBS	BS-LIBS	LIBS	BS-LIBS	LIBS	BS-LIBS	
Ore mineral	Flat-top beam	U	28.2%	15.3%	–	0.90	–	21.2	[23]
Al–Mg alloy	Flat-top beam	Mg	33%	18%	–	–	–	–	[114]
Alloyed steel	Bessel beam	Mn	39.48%	18.31%	0.933	0.956	0.34 wt.%	0.27 wt.%	[25]
Steel sample	Flat-top beam	Mn	30.17%	16.32%	0.981	0.993	**11.06**	**3.82**	[115]
		Cr	5.89%	4.69%	0.958	0.966	66.65	30.75	
Cement	Flat-top beam	Fe	2.37%	1.35%	0.9710	0.9775	56.04	29.74	[116]
		Mg			0.9936	0.9939	5.65	3.9	
		Al			0.9121	0.9166	123.51	31.63	
		Si			0.9755	0.9771	299.07	139.64	
		Na			0.9909	0.9955	7.3	2.16	
		K			0.9814	0.9889	10.6	5.67	

Sample	Beam type	*Ele.*	T(K)/FWHM*		n_e ($\times 10^{16}$ cm^{-3})		*EF*	Ref.
			LIBS	BS-LIBS	LIBS	BS-LIBS		
Ore mineral	Flat-top beam	U	–	40% ↑	–	3% ↑	**6**	[23]
Cement	Flat-top beam	Ca	**11058**	**9102**	1.29	1.04	–	[116]
Si sample	Vortex beam	Si	0.15 nm*	0.16 nm*	2.16	2.25	–	[117]
Al sample		Al	0.25 nm*	0.15 nm*	8.22	4.93		
Al–Mg alloy	Flat-top beam	Mg	**7454**	**10361**	–	–	1.5–3.5	[113]
		Al			**≈1.5**	**≈2**		

beam shaping operations, including the flat-top beam, Bessel beam, and vortex beam; both of them can reduce the *RSD* value and improve the detection limit. Besides, the plasma temperature and electron density of BS-LIBS are improved compared to SP-LIBS [23, 114]. Compared to single LIBS detection, the *LOD* value of the BS-LIBS operation can decrease by 2.9 folds [115], and the *EF* value can reach 6 folds [23].

4 Comparison and analysis

Under the LTE conditions, the integral intensity of the spectral line can be expressed as follows [118]:

$$I_{\lambda_{i,j}} = n_s A_{i,j} g_i \frac{\exp\left(-\dfrac{E_i}{k_B T(t)}\right)}{U_s(T(t))}, \tag{3}$$

where n_s is the number density (particle/cm^3) of the species s, and other parameters in the formula can refer to Eq. (1). Therefore, the spectral intensity is related to the particle density; that is, one of the important factors is the laser ablation amount or laser ablation rate. Constructing an effective laser ablation environment is beneficial for improving the *SBR*, signal-to-noise ratio (*SNR*), and *RSD* of LIBS [69, 116].

In another way, the plasma parameters of Nl, $T(t)$, and n_e can be used to characterize changes in signal intensity and uncertainty, as follows [119]:

$$\begin{aligned}\left(RSD_{I_{\lambda_{i,j}}}\right)^2 =& \frac{\sigma^2_{I_{\lambda_{i,j}}}}{{I_{\lambda_{i,j}}}^2} = \left(\frac{\partial \ln I}{\partial T(t)}\right)^2_{Nl,n_e} \sigma^2_{T(t)} \\ &+ \left(\frac{\partial \ln I}{\partial Nl}\right)^2_{T(t),n_e} \sigma^2_{Nl} + \left(\frac{\partial \ln I}{\partial n_e}\right)^2_{Nl,T(t)} \sigma^2_{n_e} \\ &+ 2\left(\frac{\partial \ln I}{\partial T(t)}\right)_{Nl,n_e} \left(\frac{\partial \ln I}{\partial Nl}\right)_{T(t),n_e} \sigma_{T(t),Nl} \\ &+ 2\left(\frac{\partial \ln I}{\partial T(t)}\right)_{Nl,n_e} \left(\frac{\partial \ln I}{\partial n_e}\right)_{Nl,T(t)} \sigma_{T(t),n_e} \\ &+ 2\left(\frac{\partial \ln I}{\partial Nl}\right)_{T(t),n_e} \left(\frac{\partial \ln I}{\partial n_e}\right)_{Nl,T(t)} \sigma_{Nl,n_e},\end{aligned} \tag{4}$$

where l is the plasma size along the line of sight, Nl (columnar total number density) is the total number density n_s time plasma size along the line of sight l. This confirmed the importance of stabilizing plasma morphology in experiments and compensating for Nl fluctuations in data processing for the reduction of signal uncertainty. By analyzing the relative contributions of plasma parameter fluctuations on the spectral signal uncertainly, the fluctuation of total number density in the plasma is the key factor influencing the signal fluctua tion during the major evolution process, and the plasma temperature fluctuation is dominant to the spectral signal fluctuation at the very early stage of the plasma evolution [32]. Further, a fundamental principle of suppressing the LIBS spectra intensity fluctuation can be understood; that is, by creating a big and stable plasma core, the observed total number density fluctuation can be suppressed, leading to a more repeatable emission line intensity. In practice, selecting the appropriate polarization direction and type or shaping the laser beam could suppress the total number density fluctuation to diminish the signal uncertainty [35, 115].

In Section 3.1, a couple of points are worth noting. First, the amount of laser ablation and spectral intensity depend on the variation of the polarization angle of linearly polarized beams [51, 52, 56, 74]. Second, the linearly polarized beam has a lower candling threshold and linewidth than the circularly polarized beam, but the latter has a longer ablation depth and spectral intensity under the same conditions. Specifically, for circularly polarized beams, because of the rotation of the laser electric field vector, phase shift changes the direction of electron collision, thus weakening the energy absorbed by multi-photon ionization in a specific direction, while for linearly polarized beams, multi-photon ionization can more effectively excite valence band bound electrons because the electric field vector does not rotate and does not cause a phase shift of valence electrons. Therefore, linearly polarized beams are greater than circularly polarized beams [66, 120, 121]. Third, the roundness and finish of the ablative holes of a vector beam are better than those of linearly and circularly polarized beams, while radial vector beams are better than angular vector beams [63]. Fourth, plasma polarization can be analyzed using LIBS quantitative analysis, but the explanation of the mechanism is inconsistent. Five opinions are presented as follows: (i) laser field effect; (ii) Fresnel diffraction effect; (iii) anisotropy of electron velocity distribution function; (iv) the effect of bremsstrahlung from dynamic ion polarization and Debye electron cloud collision; and (v) the anisotropic recombination process of plasma. Basically, most of the existing research concludes that PR-LIBS improves *SBR*, but the plasma polarization mechanisms deserve further investigation and more evidence.

In Section 3.2, beam shaping is the process of using beam control techniques to change the shape and characteristics of the beam. The biggest advantage of laser beam shaping is its ability to manipulate the intensity distribution and shape of the spot, thereby improving efficiency and quality. In the research and application of LIBS, we usually approximate the laser beam as a Gaussian beam, but LIBS typically uses lasers with high energy to enhance the emission intensity of spectral signals, while lasers are generally multi-mode excited. Compared to single-mode laser beams, the intensity distribution of multi-mode laser spots is more complex, dispersed, and has poor beam quality, as shown in Fig. 8. It can be

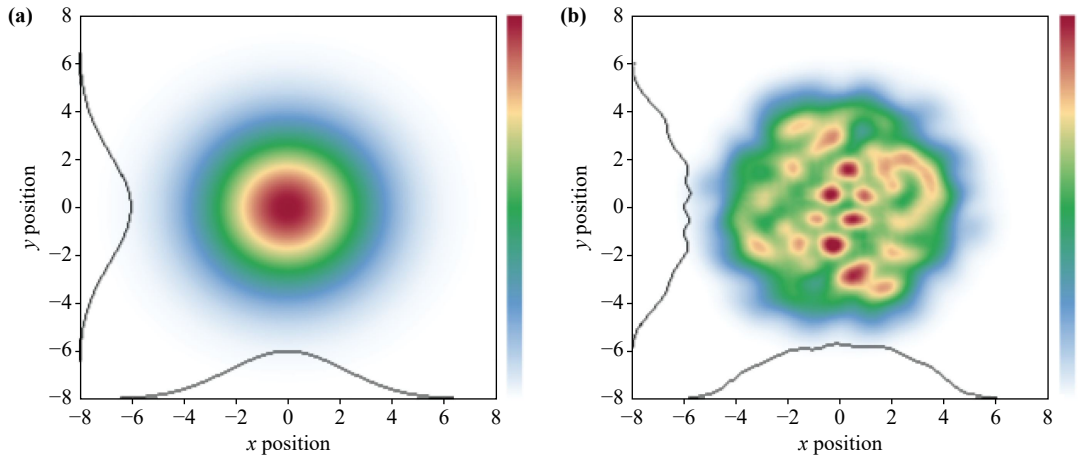

Fig. 8 **(a)** Gaussian and **(b)** multimode laser beam spots.

seen as a distribution with a strong center and weak edges, whether it is a Gaussian or multi-mode laser beam. By using a device such as beam shaping diffusers, the uneven beam of a multi-mode laser can be effectively transformed into a smooth and uniform beam, thereby improving the laser ablation state, increasing the laser ablation rate [101, 107] and *SBR/SNR* [23, 114], and decreasing the signal uncertainty. Besides, the results of laser ablation amount, plasma parameter, and quantitative analysis exhibited significant differences with different beam shaping methods, as shown in Fig. 7 and Table 3. In Fig. 7(d), the dark zones are pronounced for Gaussian and Laguerre–Gaussian pulse ablation, whereas being minimal for the Airy pulse and absent in the case of the Bessel–Gaussian pulse, the more pronounced heat-affected zones can be attributed to greater local intensity

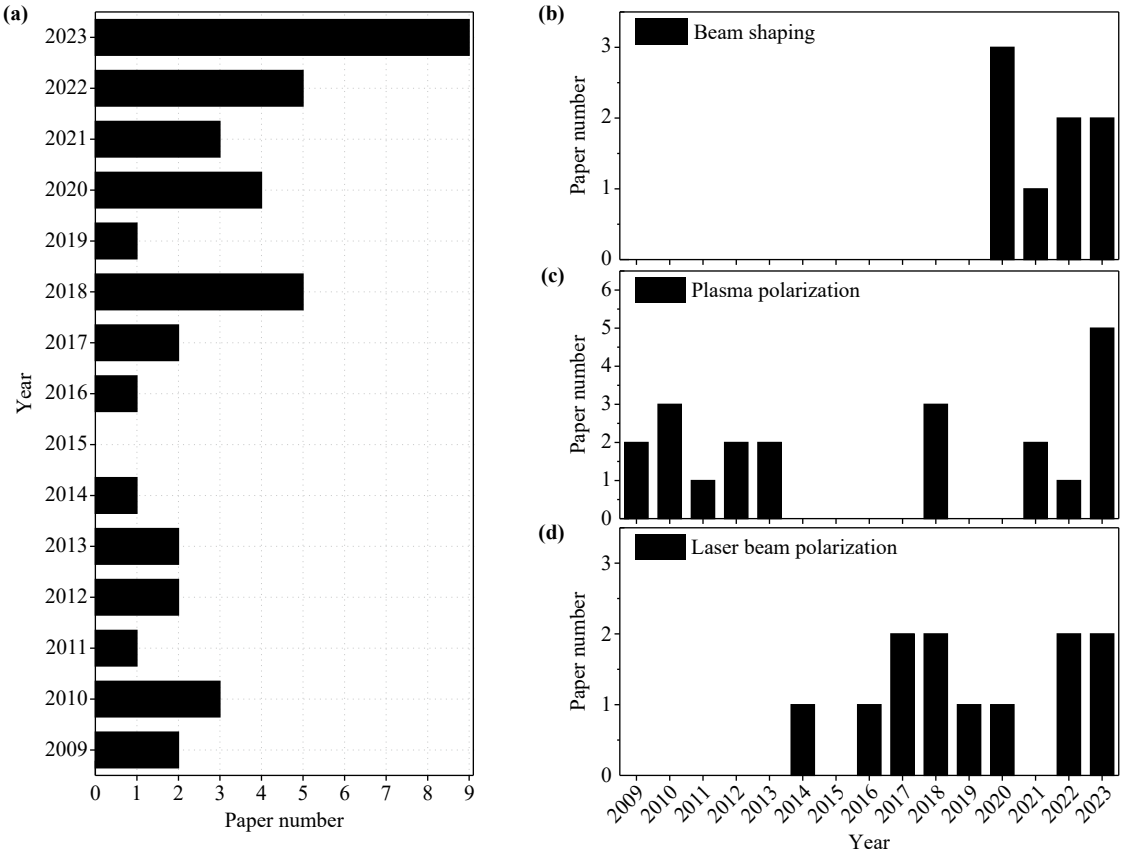

Fig. 9 Data chart of annual research article statistics with different technology types of light-field modulated LIBS, **(a)** Paper statistics in 2009–2023, **(b)** beam shaping, **(c)** plasma polarization, and **(d)** laser beam polarization.

and an increased rate of oxidation processes. Three issues need to be pointed out: (i) the difference in beam intensity distribution and laser ablation amount will lead to a difference in the intensity and distribution of plasma parameters n_s, $T(t)$, and n_e; (ii) there is a significant difference in plasma shapes, and the columnar total number density Nl is different; and (iii) there are differences in quantitative analysis ability. Based on Eq. (4), the *RSD* is related to Nl, $T(t)$ and n_e, such as the flat-top pulse-generated plasma is more uniform and brighter, which increases the spectral signal intensity and stability. Of course, this is a relatively easy conclusion to draw, but unfortunately, the current research work lacks comparison between different beam shaping methods under the same experimental conditions. We believe that more researchers will pay attention to these issues in the future.

The existence of signal uncertainty remains the biggest obstacle in LIBS quantitative chemical analysis, among which the original signal optimization is a key and difficult problem that needs to be overcome in the past, present, and future. Plasma polarization-resolved LIBS and beam shaping-assisted LIBS methods can effectively reduce *RSD* and improve signal quality [25, 35, 90, 91, 23, 114–116]. The former is based on the polarization difference between LIBS feature signals (discrete spectra) and background signals (continuous spectra), while the latter is based on improving the quality of laser beams and reducing the uncertainty of plasma radiation signals.

In this review, all of the research articles' data come from the Web of Science (WOS) open-source websites. As described in Section 3, three optimization scenarios of laser beam polarization, plasma polarization, and beam shaping are presented. The data chart of annual research article statistics with different technology types of light-field modulated LIBS is shown in Fig. 9. At the present, the emergence of such problems of signal uncertainty is seriously hampering the development and application of LIBS. The light-field modulated research is becoming greater and greater with the application requirement of LIBS since 2016. Some, especially beam shaping methods, are new technologies in the LIBS field that have developed highly in past five years.

Other optimization solutions, such as double-pulse, spark discharge pulse re-excitation, microwave supplementary, resonance excitation, and flame supplementary, require additional auxiliary devices to be equipped and have significant limitations in terms of experimental scale and application scope [122–124]. Compared to these methods, optical field modulation devices are easy to match with LIBS optical path systems and can effectively improve the quality of the LIBS signal [25, 35]. Hence, light-field modulated operation may be the most capable and low-cost way to improve LIBS quantitative abilities. Furthermore, light-field modulated LIBS combined with algorithmic model such as calibration-free model can help the achievement for further technology upgrading [125]. As light-field modulated theory and devices have increasingly matured and been completed, it is reasonable to believe that the simplicity and low-cost way to improve the qualitative and quantitative analysis performance of LIBS will appeal to more people concerned about academics, research, and application.

5 Conclusions and perspectives

With further investigation of the source of signal uncertainty in laser-produced plasma, the light-field modulated method has become an advanced research field and has caused extensive attention in recent years, especially plasma polarization and beam shaping methods, which have had very quick development and will make a very big contribution to LIBS qualitative and quantitative analysis. Light-field modulated operation can further optimize the LIBS system property, avoid background noise, shorten the system complexity, cut costs, and raise *SBR* and *RSD*. However, currently there are four problems in light-field modulation in LIBS: (i) the physical mechanism is unclear and the statements are inconsistent; (ii) the effect of background reduction and improving *SBR* varies; (iii) there is limited research on quantitative analysis, current studies have been unable to provide better supporting data; and (iv) the possibility of integrating different optimization technologies. Only after these problems were solved and obstacles surmounted could light-field modulated LIBS research and application obtain real success.

Contribution statement Shangyong Zhao: Methodology, Visualization, Investigation, Supervision, Project administration, Funding acquisition, Writing – original draft. Yuchen Zhao: Methodology, Validation, Writing – original draft & editing. Ziyuan Liu: Investigation. Yujia Dai: Investigation. Huihui Za: Writing – review & editing. Xun Gao: Supervision, Project administration, Funding acquisition.

Declarations The authors declare that they have no known competing financial interests or personal relationships that could have appeared to influence the work reported in this paper.

Acknowledgements This work was supported by the National Natural Science Foundation of China (No. 61575030) and the Scientific Research Foundation of Zhejiang A & F University, China (Nos. 2022LFR030, 2022LFR050, and 2024LFR047).

References

1. J. D. Winefordner, I. B. Gornushkin, T. Correll, E. Gibb, B. W. Smith, N. Omenetto, Comparing several atomic spectrometric methods to the superstars, special emphasis on laser induced breakdown spectrom-

etry, LIBS, a future super star, *J. Anal. Atom. Spectrom.* 19, 1061e1083 (2004)
2. Z. Wang, T. Yuan, Z. Hou, W. Zhou, J. Lu, H. Ding, and X. Zeng, Laser-induced breakdown spectroscopy in China, *Front. Phys.* 9(4), 419 (2014)
3. S. Zhao, C. Song, X. Gao, and J. Lin, Quantitative analysis of Pb in soil by femtosecond–nanosecond double-pulse laser-induced breakdown spectroscopy, *Results Phys.* 15, 102736 (2019)
4. Q. Wang, A. Chen, and X. Gao, Sensitivity improvement of laser-induced breakdown spectroscopy to detect heavy metals in water by Tesla coil discharge, *J. Anal. At. Spectrom.* 39(1), 261 (2024)
5. Y. Ikeda, J. K. Soriano, H. Ohba, and I. Wakaida, Analysis of gadolinium oxide using microwave-enhanced fiber-coupled micro-laser-induced breakdown spectroscopy, *Sci. Rep.* 13(1), 4828 (2023)
6. S. Ma, Y. Liu, H. Tian, L. Guo, and D. Dong, Investigation of resonance excitation of trace elements using resonant laser-induced breakdown spectroscopy (RLIBS), *J. Anal. At. Spectrom.* 38(2), 342 (2023)
7. Y. Song, W. Song, L. Li, W. Gu, K. Kou, M. S. Afgan, Z. Hou, Z. Li, and Z. Wang, Flame-assisted plasma modulation to improve the raw signal quality for laser-induced breakdown spectroscopy, *Opt. Lasers Eng.* 162, 107433 (2023)
8. S. Zhao, X. Gao, A. Chen, and J. Lin, Effect of spatial confinement on Pb measurements in soil by femtosecond laser-induced breakdown spectroscopy, *Appl. Phys. B* 126(1), 7 (2020)
9. M. A. Khan, S. Bashir, N. A. Chishti, E. Bonyah, A. Dawood, and Z. Ahmad, Effect of ambient environment and magnetic field on laser-induced cobalt plasma, *AIP Adv.* 13(1), 015017 (2023)
10. Q. Wang, Y. Liu, L. Jiang, A. Chen, J. Han, and M. Jin, Metal micro/nanostructure enhanced laser-induced breakdown spectroscopy, *Anal. Chim. Acta* 1241, 340802 (2023)
11. Y. Zhu, N. Deng, Z. Hu, W. Wang, C. Lau, Y. Liu, and L. Guo, Droplet constraint by a superhydrophobic –superhydrophilic hybrid surface with a SiO_2 NP coating for determination of heavy metals using LIBS, *ACS Appl. Nano Mater.* 5(12), 17508 (2022)
12. J. Yu, Z. Hou, Y. Ma, T. Li, Y. Fu, Y. Wang, Z. Li, and Z. Wang, Improvement of laser induced breakdown spectroscopy signal using gas mixture, *Spectrochim. Acta B* 174, 105992 (2020)
13. K. Zehra, S. Bashir, S. A. Hassan, Q. S. Ahmed, M. Akram, and A. Hayat, The effect of nature and pressure of ambient environment on laser-induced breakdown spectroscopy and ablation mechanisms of Si, *Laser Part. Beams* 35(3), 492 (2017)
14. Y. Zhao, S. Singha, Y. Liu, and R. J. Gordon, Polarization-resolved laser-induced breakdown spectroscopy, *Opt. Lett.* 34(4), 494 (2009)
15. Y. Liu, J. S. Penczak, and R. J. Gordon, Nanosecond polarization-resolved laser-induced breakdown spectroscopy, *Opt. Lett.* 35(2), 112 (2010)
16. L. Nagli and M. Gaft, Fraunhofer-type absorption line splitting and polarization in confocal double-pulse laser induced plasma, *Spectrochim. Acta B* 88, 127 (2013)
17. S. Sheta, Z. Hou, Y. Wang, and Z. Wang, Evaluation of femtosecond laser-induced breakdown spectroscopy system as an offline coal analyzer, *Sci. Rep.* 11(1), 15968 (2021)
18. S. Ma, L. Guo, and D. Dong, A molecular laser-induced breakdown spectroscopy technique for the detection of nitrogen in water, *J. Anal. At. Spectrom.* 37(3), 663 (2022)
19. W. Wang, L. Sun, G. Wang, P. Zhang, L. Qi, L. Zheng, and W. Dong, The effect of sample surface roughness on microanalysis of microchip laser-induced breakdown spectroscopy, *J. Anal. At. Spectrom.* 35(2), 357 (2020)
20. R. Liu, K. Rong, Z. Wang, M. Cui, Y. Deguchi, S. Tanaka, J. Yan, and J. Liu, Sample temperature effect on steel measurement using SP-LIBS and collinear long-short DP-LIBS, *ISIJ Int.* 60(8), 1724 (2020)
21. F. Poggialini, B. Campanella, S. Legnaioli, S. Pagnotta, and V. Palleschi, Investigating double pulse nanoparticle enhanced laser induced breakdown spectroscopy, *Spectrochim. Acta B* 167, 105845 (2020)
22. H. Li, C. Wang, Y. Wang, S. Fu, and L. Fang, Double-enhanced LIBS system with N_2 atmosphere and cylindrical cavity confinement for quantitative analysis of Sr element in soil, *Meas. Sci. Technol.* 34(9), 095204 (2023)
23. J. Ji, W. Song, Z. Hou, L. Li, X. Yu, and Z. Wang, Raw signal improvement using beam shaping plasma modulation for uranium detection in ore using laser-induced breakdown spectroscopy, *Anal. Chim. Acta* 1235, 340551 (2022)
24. J. Gao, J. Yang, Z. Wang, S. Sun, B. Hu, and Z. Liu, The study of femtosecond LIBS in Vortex–Gaussian and double Gaussian configurations, *Appl. Phys. B* 129(8), 119 (2023)
25. J. Lv, C. Zhu, Z. Tang, Q. Li, K. Liu, W. Zhang, K. Liu, and X. Li, Bessel beams: A potential strategy for laser-induced breakdown spectroscopy, *J. Anal. At. Spectrom.* 36(12), 2756 (2021)
26. M. Hu, S. Shi, M. Yan, E. Wu, and H. Zeng, Femtosecond laser-induced breakdown spectroscopy by multidimensional plasma grating, *J. Anal. At. Spectrom.* 37(4), 841 (2022)
27. U. K. Adarsh, V. K. Unnikrishnan, P. Vasa, S. D. George, S. Chidangil, and D. Mathur, Effect of laser polarization on atomic and ionic emissions in laser-induced breakdown spectroscopy (LIBS), *Appl. Phys. B* 129(12), 185 (2023)
28. L. Yang, M. Liu, Y. Liu, Q. Li, S. Li, Y. Jiang, A. Chen, and M. Jin, Influence of polarization of laser beam on emission intensity of femtosecond laser-induced breakdown spectroscopy, *Chin. Phys. B* 29(6), 065203 (2020)
29. S. Zhao, Y. Zhao, Z. Hou, and Z. Wang, Rapid and high-resolution visualization elements analysis of material surface based on laser-induced breakdown spectroscopy and hyperspectral imaging, *Appl. Surf. Sci.* 629, 157415 (2023)
30. S. Zhao, C. Song, X. Gao, K. Guo, Z. Hao, and J. Lin, The plasma characteristics of femtosecond–nanosecond dual–pulse laser ablated soil, *Results Phys.* 19, 103601

(2020)
31. P. S. Hsu, A. K. Patnaik, A. J. Stolt, J. Estevadeordal, S. Roy, and J. R. Gord, Femtosecond-laser-induced plasma spectroscopy for high-pressure gas sensing: Enhanced stability of spectroscopic signal, *Appl. Phys. Lett.* 113(21), 214103 (2018)
32. Y. Fu, Z. Hou, T. Li, Z. Li, and Z. Wang, Investigation of intrinsic origins of the signal uncertainty for laser-induced breakdown spectroscopy, *Spectrochim. Acta B* 155, 67 (2019)
33. Y. Fu, W. Gu, Z. Hou, S. A. Muhammed, T. Li, Y. Wang, and Z. Wang, Mechanism of signal uncertainty generation for laser-induced breakdown spectroscopy, *Front. Phys.* 16(2), 22502 (2021)
34. T. A. Labutin, V. N. Lednev, A. A. Ilyin, and A. M. Popov, AM, Femtosecond laser-induced breakdown spectroscopy, *J. Anal. At. Spectrom.* 31(1), 90 (2016)
35. S. Zhao, Y. Zhao, Z. Hou, and Z. Wang, Stability and accuracy improvement of element analysis in steel alloys using polarization-resolved laser-induced breakdown spectroscopy, *Spectrochim. Acta B* 203, 106666 (2023)
36. Z. Wang, M. S. Afgan, W. L. Gu, Y. Z. Song, Y. Wang, Z. Y. Hou, W. R. Song, and Z. Li, Recent advances in laser-induced breakdown spectroscopy quantification: From fundamental understanding to data processing, *Trends Analyt. Chem.* 143, 116385 (2021)
37. H. Le, P. Penchev, A. Henrottin, D. Bruneel, V. Nasrollahi, J. A. Ramos-de-Campos, and S. Dimov, Effects of top-hat laser beam processing and scanning strategies in laser micro-structuring, *Micromachines (Basel)* 11(2), 221 (2020)
38. C. Liu and Y. Guo, Flat-top line-shaped beam shaping and system design, *Sensors* 22(11), 4199 (2022)
39. M. A. Poletti, Spherical coordinate descriptions of cylindrical and spherical Bessel beams, *J. Acoust. Soc. Am.* 141(3), 2069 (2017)
40. X. Zhao and X. Jia, Vectorial structure of arbitrary vector vortex beams diffracted by a circular aperture in the far field, *Laser Phys.* 28(1), 015004 (2018)
41. Z. Zhang, S. Wang, X. Hu, S. Wang, Y. Pu, H. Li, and J. Wang, All-fiber passively Q-switched laser with flat-top beam emissions, *Opt. Lett.* 47(3), 521 (2022)
42. V. K. Unnikrishnan, K. Alti, V. B. Kartha, C. Santhosh, G. P. Gupta, and B. M. Suri, Measurements of plasma temperature and electron density in laser-induced copper plasma by time-resolved spectroscopy of neutral atom and ion emissions, *Pramana* 74(6), 983 (2010)
43. B. Man, Q. Dong, A. Liu, X. Wei, Q. Zhang, J. He, and X. Wang, Line-broadening analysis of plasma emission produced by laser ablation of metal Cu, *J. Opt. A* 6(1), 17 (2004)
44. J. Wang, X. Li, H. Li, X. Li, and Z. Li, Lens-to-sample distance effect on the quantitative analysis of steel by laser-induced breakdown spectroscopy, *J. Phys. D* 53(25), 255203 (2020)
45. H. Yin, Z. Hou, T. Yuan, Z. Wang, W. Ni, and Z. Li, Application of spatial confinement for gas analysis using laser-induced breakdown spectroscopy to improve signal stability, *J. Anal. At. Spectrom.* 30(4), 922 (2015)
46. W. Song, Z. Song, J. Vincent, H. Wang, and Z. Wang, Quantification of extra virgin olive oil adulteration using smartphone videos, *Talanta* 216, 120920 (2020)
47. C. L. Goueguel, A. Soumare, C. Nault, and J. Nault, Direct determination of soil texture using laser-induced breakdown spectroscopy and multivariate linear regressions, *J. Anal. At. Spectrom.* 34(8), 1588 (2019)
48. C. R. Bhatt, D. Hartzler, J. C. Jain, and D. L. McIntyre, Evaluation of analytical performance of double pulse laser-induced breakdown spectroscopy for the detection of rare earth elements, *Opt. Laser Technol.* 126, 106110 (2020)
49. E. M. Garcell and C. Guo, Polarization-controlled microgroove arrays induced by femtosecond laser pulses, *J. Appl. Phys.* 123(21), 213103 (2018)
50. X. Li, W. Rong, L. Jiang, K. Zhang, C. Li, Q. Cao, G. Zhang, and Y. Lu, Generation and elimination of polarization dependent ablation of cubic crystals by femtosecond laser radiation, *Opt. Express* 22(24), 30170 (2014)
51. X. Ji, L. Jiang, X. Li, W. Han, Y. Liu, Q. Huang, and Y. Lu, Polarization-dependent elliptical crater morphologies formed on a silicon surface by single-shot femtosecond laser ablation, *Appl. Opt.* 53(29), 6742 (2014)
52. S. M. Pimenov, E. V. Zavedeev, B. Jaeggi, and B. Neuenschwander, Femtosecond laser-induced periodic surface structures in titanium-doped diamond-like nanocomposite films: Effects of the beam polarization rotation, *Materials (Basel)* 16(2), 795 (2023)
53. F. Bai, H. Li, Y. Huang, W. Fan, H. Pan, Z. Wang, C. Wang, J. Qian, Y. Li, and Q. Zhao, Polarization effects in femtosecond laser induced amorphization of monocrystalline silicon, *Chem. Phys. Lett.* 662, 102 (2016)
54. G. K. Krasin, M. S. Kovalev, S. I. Kudryashov, P. A. Danilov, V. P. Martovitskii, I. V. Gritsenko, I. M. Podlesnykh, R. A. Khmelnitskii, E. V. Kuzmin, Y. S. Gulina, and A. O. Levchenko, Polarization-dependent near-IR ultrashort-pulse laser ablation of natural diamond surfaces, *Appl. Surf. Sci.* 595, 153549 (2022)
55. V. Wanie, T. Shao, P. Lassonde, F. Calegari, F. Vidal, H. Ibrahim, X. Bian, and F. Légaré, Laser polarization dependence of strong-field ionization in lithium niobate, *Phys. Rev. B* 101(21), 214311 (2020)
56. X. Liu, W. Cheng, M. Petrarca, and P. Polynkin, Universal threshold for femtosecond laser ablation with oblique illumination, *Appl. Phys. Lett.* 109(16), 161604 (2016)
57. J. M. Guay, A. Villafranca, F. Baset, K. Popov, L. Ramunno, and V. R. Bhardwaj, Polarization-dependent femtosecond laser ablation of poly-methyl methacrylate, *New J. Phys.* 14(8), 085010 (2012)
58. J. A. Tomko, R. Jimenez, J. J. Naddeo, D. M. Bubb, and S. M. O'Malley, Effects of laser polarization and linear surface features on nanoparticle synthesis during laser ablation in liquids, *Laser Phys.* 28(3), 035602 (2018)

59. Y. Liu, A. Gruner, D. G. K. Aboud, J. Bonse, J. Schille, U. Loeschner, and A. M. Kietzig, Polarization effects on laser-inscribed angled micro-structures, *Appl. Surf. Sci.* 649, 159191 (2024)
60. S. Shin, J. Hur, J. K. Park, and D. Kim, Polarization effects on ablation efficiency and microstructure symmetricity in femtosecond laser processing of materials — developing a pattern generation model for laser scanning, *Opt. Express* 30(11), 18018 (2022)
61. H. Cheng, P. Li, S. Liu, H. Lu, L. Han, and J. Zhao, Polarization-switchable nanoripples fabricated on a silicon surface by femtosecond-laser-assisted nanopatterning, *Appl. Opt.* 59(24), 7211 (2020)
62. G. Lazzini, L. Romoli, F. Tantussi, and F. Fuso, Nanostructure patterns on stainless-steel upon ultrafast laser ablation with circular polarization, *Opt. Laser Technol.* 107, 435 (2018)
63. Y. Guo, P. Qiu, and S. Xu, Combined effects of polarization and secondary ablation on precision machining of microgrooves by laser-induced microjet-assisted ablation, *Opt. Express* 30(25), 44665 (2022)
64. R. Torres, T. Kaempfe, M. Delaigue, O. Parriaux, C. Hoenninger, J. Lopez, R. Kling, and E. Mottay, Influence of laser beam polarization on laser micro-machining of molybdenum, *J. Laser Micro Nanoeng.* 8(3), 188 (2013)
65. V. N. Lednev, S. M. Pershin, A. A. Ionin, S. I. Kudryashov, S. V. Makarov, A. E. Ligachev, A. A. Rudenko, R. A. Chmelnitsky, and A. F. Bunkin, Laser ablation of polished and nanostructured titanium surfaces by nanosecond laser pulses, *Spectrochim. Acta B* 88, 15 (2013)
66. H. Al-Khazraji and V. R. Bhardwaj, Polarization dependent micro-structuring of silicon with a femtosecond laser, *Appl. Surf. Sci.* 353, 600 (2015)
67. H. Guo, Z. Zhu, T. Wang, N. Chen, Y. Liu, J. Zhang, H. Sun, J. Liu, and R. Li, Polarization-gated filament-induced remote breakdown spectroscopy, *Chin. Opt. Lett.* 16(3), 033201 (2018)
68. J. Hou, L. Zhang, W. Yin, Y. Zhao, W. Ma, L. Dong, G. Yang, L. Xiao, and S. Ji, Investigation on spatial distribution of optically thin condition in laser-induced aluminum plasma and its relationship with temporal evolution of plasma characteristics, *J. Anal. At. Spectrom.* 32(8), 1519 (2017)
69. Q. Wang, A. Chen, Y. Wang, L. Sui, S. Li, and M. Jin, Spectral intensity clamping in linearly and circularly polarized femtosecond filament-induced Cu plasmas, *J. Anal. At. Spectrom.* 33(7), 1154 (2018)
70. Q. Wang, A. Chen, X. Wang, S. Li, J. Jiang, and M. Jin, Signal improvement using circular polarization for focused femtosecond laser-induced breakdown spectroscopy, *J. Anal. At. Spectrom.* 34(6), 1242 (2019)
71. S. Li, Y. Jiang, A. Chen, L. He, D. Liu, and M. Jin, Revisiting the mechanism of nitrogen fluorescence emission induced by femtosecond filament in air, *Phys. Plasmas* 24(3), 033111 (2017)
72. Y. Chen, Y. Liu, Q. Wang, S. Li, Y. Jiang, A. Chen, and M. Jin, Effect of laser polarization on molecular emission from femtosecond LIBS, *J. Anal. At. Spectrom.* 37(1), 82 (2022)
73. G. A. Wubetu, J. T. Costello, T. J. Kelly, P. Wachulak, A. Bartnik, W. Skrzeczanowski, and H. Fiedorowicz, Comparison of LIBS and polarization resolved LIBS emission for aluminium alloy, *J. Appl. Spectrosc.* 90(1), 116 (2023)
74. Y. Shi, A. Chen, Y. Jiang, S. Li, and M. Jin, Influence of laser polarization on plasma fluorescence emission during the femtosecond filamentation in air, *Opt. Commun.* 367, 174 (2016)
75. D. Zhao, N. Farid, R. Hai, D. Wu, and H. Ding, Diagnostics of First Wall Materials in a Magnetically Confined Fusion Device by Polarization-Resolved Laser-Induced Breakdown Spectroscopy, *Plasma Sci. Technol.* 16(2), 149 (2014)
76. J. Xu, X. Wang, and M. Yao, Optimization of copper detection based on polarization-resolved laser-induced breakdown spectroscopy, *Appl. Opt.* 60(17), 5266 (2021)
77. X. Wang, M. Yao, M. Zeng, and J. Xu, Detection model of copper based on polarization degree induced by low-energy density laser, *Appl. Opt.* 60(35), 10780 (2021)
78. J. S. Penczak, Y. Liu, and R. J. Gordon, Polarization and fluence dependence of the polarized emission in nanosecond laser-induced breakdown spectroscopy, *Spectrochim. Acta B* 66(2), 186 (2011)
79. J. Xu, X. Wang, M. Yao, and M. Liu, Detection model of the plasma spectrum based on the polarization recognition rate induced by a low energy density laser, *Appl. Opt.* 61(16), 4768 (2022)
80. A. Eslami Majd, A. S. Arabanian, and R. Massudi, Polarization resolved laser induced breakdown spectroscopy by single shot nanosecond pulsed Nd: YAG laser, *Opt. Lasers Eng.* 48(7-8), 750 (2010)
81. N. Agnes, H. Y. Tao, Z. Q. Hao, C. K. Sun, X. Gao, and J. Q. Lin, A comparison of single shot nanosecond and femtosecond polarization-resolved laser-induced breakdown spectroscopy of Al, *Chin. Phys. B* 22(1), 014209 (2013)
82. M. Aghababaei Nejad, M. Soltanolkotabi, and A. Eslami Majd, Polarization investigation of laser-induced breakdown plasma emission from Al, Cu, Mo, W, and Pb elements using nongated detector, *J. Laser Appl.* 30(2), 022005 (2018)
83. J. S. Penczak, Y. Liu, and R. J. Gordon, Polarization resolved laser-induced breakdown spectroscopy of Al, *J. Phys. Chem. A* 113(47), 13310 (2009)
84. M. E. Asgill, H. Y. Moon, N. Omenetto, and D. W. Hahn, Investigation of polarization effects for nanosecond laser-induced breakdown spectroscopy, *Spectrochim. Acta B* 65(12), 1033 (2010)
85. E. Yurdanur-Tasel, H. Berberoglu, and S. Bilikmen, Investigation of materials of different crystal structure under various time delays using double pulse laser induced breakdown spectroscopy, *Spectrochim. Acta B* 74–75, 74 (2012)
86. Y. Jr Penczak, R. D. Liu, D. H. Schaller, Rich, and R. J. Gordon, The mechanism for continuum polarization in laser induced breakdown spectroscopy of Si (111), *Spectrochim. Acta B* 74–75, 3 (2012)
87. M. Aghababaei Nejad, and A. Eslami Majd, Temporal

evolution of polarization resolved laser-induced breakdown spectroscopy of Cu, *Plasma Chem. Plasma Process.* 40(1), 325 (2020)
88. A. P. Williamson, and J. Kiefer, Strategies for suppressing elastically scattered laser light in ungated laser-induced breakdown spectroscopy, *Spectrochim. Acta B* 149, 267 (2018)
89. M. Aghababaei Nejad, M. Soltanolkotabi, and A. Eslami Majd, Polarization mechanism in a ns laser-induced plasma spectroscopy of Al alloy, *Appl. Phys. B* 124(1), 6 (2018)
90. H. Zhao, L. Cai, and G. Wu, On polarization resolved laser induced breakdown spectroscopy combined with support-vector regression to improve the accuracy of soil heavy-metal (Cd) detection, *Chin. J. Anal. Chem.* 51(2), 100176 (2023)
91. J. Xu, X. Wang, M. Yao, and M. Liu, Improving the stability of LIBS for chromium in soil based on the model of micro-linear spectrum, *J. Anal. At. Spectrom.* 38(11), 2441 (2023)
92. G. Teng, Q. Wang, Q. Hao, A. Fan, H. Yang, X. Xu, G. Chen, K. Wei, Z. Zhao, M. N. Khan, B. S. Idrees, M. Bao, T. Luo, Y. Zheng, and B. Lu, Full-Stokes polarization laser-induced breakdown spectroscopy detection of infiltrative glioma boundary tissue, *Biomed. Opt. Express* 14(7), 3469 (2023)
93. J. Li, Y. Tang, Z. Kuang, J. Schille, U. Loeschner, W. Perrie, D. Liu, G. Dearden, and S. Edwardson, Multi imaging-based beam shaping for ultrafast laser-material processing using spatial light modulators, *Opt. Lasers Eng.* 112, 59 (2019)
94. S. Rung, J. Barth, and R. Hellmann, Characterization of laser beam shaping optics based on their ablation geometry of thin films, *Micromachines (Basel)* 5(4), 943 (2014)
95. K. K. Anoop, A. Rubano, R. Fittipaldi, X. Wang, D. Paparo, A. Vecchione, L. Marrucci, R. Bruzzese, and S. Amoruso, Femtosecond laser surface structuring of silicon using optical vortex beams generated by a q-plate, *Appl. Phys. Lett.* 104(24), 241604 (2014)
96. D. Kong, X. Sun, Y. Hu, and J. Duan, Theoretical and experimental research on a spatially modulated femtosecond bessel-like laser for microdrilling in silica glass, *Opt. Commun.* 542, 129594 (2023)
97. L. Ackermann, M. Gehring, C. Roider, K. Cvecek, and M. Schmidt, Spot arrays for uniform material ablation with ultrashort pulsed lasers, *Opt. Laser Technol.* 163, 109358 (2023)
98. D. Doan, R. Iida, B. Kim, I. Satoh, and K. Fushinobu, Bessel beam laser-scribing of thin film silicon solar cells by ns pulsed laser, *J. Therm. Sci. Tech.* 11(1), JTST0011 (2016)
99. R. Sahin and I. Kabacelik, Nanostructuring of ITO thin films through femtosecond laser ablation, *Appl. Phys. A* 122(4), 314 (2016)
100. P. Yin, B. Xu, Y. Liu, Y. Wang, W. Zhao, and J. Tang, Simulation of evaporation ablation dynamics of materials by nanosecond pulse laser of Gaussian beam and flat-top beam, *Acta Phys. Sin.* 73(9), 095202 (2024)
101. J. Choi, W. Choi, Y. Shin, S. Han, K. Kim, and S. Cho, Enhancement periodic regularity of surface nano ripple structures on Si wafer using a square shaped flat-top beam femtosecond NIR laser, *Appl. Phys. A* 128(1), 46 (2022)
102. M. Burger, P. Polynkin, and I. Jovanovic, Filament-induced breakdown spectroscopy with structured beams, *Opt. Express* 28(24), 36812 (2020)
103. E. Figueiras, D. Olivieri, A. Paredes, and H. Michinel, An open source virtual laboratory for the Schrödinger equation, *Eur. J. Phys.* 39(5), 055802 (2018)
104. L. Ackermann, C. Roider, K. Cvecek, and M. Schmidt, Methods for uniform beam shaping and their effect on material ablation, *Appl. Phys. A* 128(10), 877 (2022)
105. D. Pallarés-Aldeiturriaga, A. Abou Khalil, J. P. Colombier, R. Stoian, and X. Sedao, Ultrafast Cylindrical Vector Beams for Improved Energy Feedthrough and Low Roughness Surface Ablation of Metals, *Materials (Basel)* 16(1), 176 (2022)
106. H. Kim, J. Yoon, W. Choi, K. Kim, and S. Cho, Ablation depth control with 40 nm resolution on ITO thin films using a square, flat top beam shaped femtosecond NIR laser, *Opt. Lasers Eng.* 84, 44 (2016)
107. Z. Kuang, J. Li, S. Edwardson, W. Perrie, D. Liu, and G. Dearden, Ultrafast laser beam shaping for material processing at imaging plane by geometric masks using a spatial light modulator, *Opt. Lasers Eng.* 70, 1 (2015)
108. Y. Shin, J. Choi, and S. Cho, Fine ablation with depth control of 25-nm resolution and morphologies irradiated by femtosecond laser pulses via beam shaping, *Appl. Phys. A* 129(8), 534 (2023)
109. D. Liu, Y. Wang, Z. Zhai, Z. Fang, Q. Tao, W. Perrie, S. P. Edwarson, and G. Dearden, Dynamic laser beam shaping for material processing using hybrid holograms, *Opt. Laser Technol.* 102, 68 (2018)
110. R. Sahin, T. Ersoy, and S. Akturk, Ablation of metal thin films using femtosecond laser Bessel vortex beams, *Appl. Phys. A* 118(1), 125 (2015)
111. T. Häfner, J. Strauß, C. Roider, J. Heberle, and M. Schmidt, Tailored laser beam shaping for efficient and accurate microstructuring, *Appl. Phys. A* 124(2), 111 (2018)
112. D. Zhang, X. Li, Y. Fu, Q. Yao, Z. Li, and K. Sugioka, Liquid vortexes and flows induced by femtosecond laser ablation in liquid governing formation of circular and crisscross LIPSS, *Opto-Electron. Adv.* 5(2), 210066 (2022)
113. W. Yan, J. Lv, C. Zhu, Q. Li, J. Chen, L. Kang, B. Lu, and X. Li, Classification of uneven steel samples by laser induced breakdown spectroscopy based on a Bessel beam, *J. Anal. At. Spectrom.* 38(6), 1232 (2023)
114. Z. Hou, M. S. Afgan, S. Sheta, J. Liu, and Z. Wang, Plasma modulation using beam shaping to improve signal quality for laser induced breakdown spectroscopy, *J. Anal. At. Spectrom.* 35(8), 1671 (2020)
115. J. Jia, H. Fu, Z. Hou, H. Wang, Z. Wang, F. Dong, Z. Ni, and Z. Zhang, Effect of laser beam shaping on the determination of manganese and chromium elements in steel samples using laser-induced breakdown spectroscopy, *Spectrochim. Acta B* 163, 105747 (2020)
116. J. Jia, H. Fu, Z. Hou, H. Wang, Z. Ni, Z. Wang, F.

Dong, and Z. Zhang, Analysis of element content in cement by Gaussian and flattop laser-induced breakdown spectroscopy, *J. Phys. D* 52(40), 405102 (2019)
117. J. Gao, J. Yang, Z. Wang, S. Sun, B. Hu, and Z. Liu, The study of femtosecond LIBS in Vortex–Gaussian and double Gaussian configurations, *Appl. Phys. B* 129(8), 119 (2023)
118. A. Ciucci, M. Corsi, V. Palleschi, S. Rastelli, A. Salvetti, and E. Tognoni, New procedure for quantitative elemental analysis by laser-induced plasma spectroscopy, *Appl. Spectrosc.* 53(8), 960 (1999)
119. W. Gu, N. Nishi, Z. Hou, Z. Wang, and T. Sakka, Investigation of the signal uncertainty in laser-induced breakdown spectroscopy based on error propagation considering self-absorption, *Spectrochim. Acta B* 206, 106732 (2023)
120. A. P. Joglekar, H. Liu, G. J. Spooner, E. Meyhöfer, G. Mourou, and A. J. Hunt, A study of the deterministic character of optical damage by femtosecond laser pulses and applications to nanomachining, *Appl. Phys. B* 77(1), 25 (2003)
121. V. V. Temnov, K. Sokolowski-Tinten, P. Zhou, A. El-Khamhawy, and D. von der Linde, Multiphoton ionization in dielectrics: Comparison of circular and linear polarization, *Phys. Rev. Lett.* 97(23), 237403 (2006)
122. K. Zhang, W. Song, Z. Hou, and Z. Wang, Effect of ambient pressures on laser-induced breakdown spectroscopy signals, *Front. Phys.* 19(4), 42203 (2024)
123. L. Guo, D. Zhang, L. Sun, S. Yao, L. Zhang, Z. Wang, Q. Wang, H. Ding, Y. Lu, Z. Hou, and Z. Wang, Development in the application of laser-induced breakdown spectroscopy in recent years: A review, *Front. Phys.* 16(2), 22500 (2021)
124. Z. Wang, Y. Deguchi, Z. Zhang, Z. Wang, X. Zeng, and J. Yan, Laser-induced breakdown spectroscopy in Asia, *Front. Phys.* 11(6), 114213 (2016)
125. Z. Hou, W. Gu, T. Li, Z. Wang, L. Li, X. Yu, Y. Zhang, and Z. Liu, A calibration-free model for laser-induced breakdown spectroscopy using non-gated detectors, *Front. Phys.* 17(6), 62503 (2022)